Vortical Modeling in the DLR TAU Code

K.A. Weinman

Abstract. Boussinesq-type closures for the Reynolds Averaged Navier-Stokes (RANS) equations fail to correctly predict Reynolds stress components for flow over curved surfaces and flow in rotating fluids [2], [33]. Two classes of vortical correction (VC) model are discussed with respect to the improvements in the predictive capability of RANS they offer for flows where substantial streamline curvature/rotation effects exist. The work is intended to improve the fidelity of vortical flow computations within the RANS/URANS modeling framework of the DLR TAU code.

1 Introduction

Correct modeling of vortical flow, for example correct prediction of a trailing vortex system, is essential to estimate induced drag and lift on lifting systems. Several models which attempt to improve vortical flow modeling are implemented in the DLR TAU code [23]. These models are evaluated within the context of attached boundary layer flow with and without curvature effects, and for more complex 2D/3D aerodynamic configurations.

2 The Numerical Method

The DLR TAU code uses a finite volume scheme to solve the conservation form of the compressible Navier-Stokes equations with additional transport equations for turbulence modeling and scalar transport. Integration in time is achieved using second and higher order Runge-Kutta schemes or an implicit LU-SGS implicit scheme [10]. A full description of the code can be found in [23].

K.A. Weinman
DLR, Bunsenstr.10, Göttingen 37073, Germany
e-mail: keith.weinman@dlr.de

A. Dillmann et al. (Eds.): *New Results in Numer. & Exp. Fluid Mech.*, NNFM 121, pp. 439–446.
DOI: 10.1007/978-3-642-35680-3_52

3 Transformation Properties of the Navier-Stokes Equations

The Navier-Stokes equations satisfy certain symmetry conditions: Reynolds number similarity, invariance under fixed rotation and reflection, invariance in different inertial reference frames (Galilean invariance), but lack invariance under a general frame rotation [19]. For example, a vector that is constant in an inertial reference frame will rotate in time relative to a non-inertial frame giving rise to explicit contributions of the frame rotation to the turbulent shear stress transport terms [19]. Scalar transport models only consider frame rotation through the absolute vorticity - explicit contributions of frame rotation to the production of the Reynolds stress are ignored [9]. Vortical correction models attempt to redress this weakness.

4 Modeling Vortical Flow

The velocity gradient $u_{i,j}$ forms a component of a second-order tensor which can be decomposed into isotropic, symmetric, and anti-symmetric parts [9], [19]. The dilation $u_{i,i}$ is zero for constant density flows, the symmetric rate-of-strain tensor is given by $S_{ij} = 0.5(u_{i,j} + u_{j,i}) - \frac{1}{3}\delta_{ij}u_{k,k}$ where δ_{ij} is the Kronecker's delta [26], and the anti-symmetric rate-of-rotation tensor is $\Omega_{ij} = 0.5(u_{i,j} - u_{j,i})$. The symmetric and anti-symmetric invariants are given by $S^2 = 2S_{ij}S_{ij}$ and $W^2 = 2W_{ij}W_{ij}$. Let the ratio of the invariants S and W be denoted by $r^\star = S/W$. For eddy-viscosity transport models (EVM's), frame rotation terms are removed via contraction on the Reynolds stress transport equation and, as a consequence, EVM's based on the turbulent energy equation are not naturally sensitive to curvature effects. In a two-dimensional flow, a Galilean-invariant measure of rotation and curvature can be obtained by comparing S and the vorticity magnitude Ω_z [29]. In an attached boundary layer the difference between S and Ω_z is small: the choice of an appropriate universal calibration coefficient [29] is problematic. Since the turbulent eddy-viscosity is proportional to a turbulent length scale, the length scale can be re-scaled by $r^\star$ [12]. The models implemented in TAU which use $r^\star$ to provide a curvature/rotation sensor are listed in table 1. A more complex class of models, where the principal strain axes are tracked w.r.t. an inertial reference frame, was first suggested by [14] with a more general extension being proposed by [29]. Differences between the Spalart-Allmaras version of this model [27] and the Menter-SST form [24] are listed in table 2.

Table 1 Vortical correction models using only $r^\star$ as a flow curvature/rotation sensor

Sym.	Turb. Model	Ref.	Mod.	Model	C	Default value
F	SA	[7]	$f_r P_{SA}$	$f_r = [1 + C\min(r^\star - 1, 0)]$	$[3.5 - 4.0]$	3.6
H	$k-\omega$	[12]	$f_r D_\omega$	$f_r = 1/(1 + CR_i)$	$[2.6 - 3.6]$	3.6
K	$k-\omega$	[4]	$f_r P_\omega$	$f_r = 1/\min(1, r^{\star 2})$	-	-

Table 2 Vortical correction models based on [29]. The coefficients C_i are described in [27].

Symbol	Turb. Model.	Ref.	Mod.	C_1	C_2	C_3
S	SA	[27]	$f_r P_{(SA)}$	1	12	[0.56, 1.]
S	$k-\omega$	[24]	$f_r P_{(k)}$, $f_r P_{(\omega)}$	1	12	[0.56, 1.]

5 Turbulence Models

Turbulence transport equations within an Eulerian framework are convection-diffusion equations with source terms for the production (P) and destruction (D) of the respective turbulence variables. VC model calculations are based on two different base turbulence models: the Spalart-Allmaras (SA) model [28], [31] and the Menter SST (SST) model [15], [31], [33]. Modifications to the turbulence model production and destruction terms are listed in tables 1 and 2.

6 Assessment of Model Response to Rotation/Curvature

A two-dimensional zero-pressure gradient flat plate (ZPGFP) computation was performed to verify that VC models remain passive where curvature/rotation effects can be ignored. The hexahedral mesh used was sufficiently fine to return maximum value of y^+ of the order of O(1.5) for all calculations. Boundary conditions were specified according to [21]. The skin friction profiles returned by the models were compared against each other and against the experiment of [32] and the theoretical estimate given by $c_f = 0.025 Re_x^{-1/7}$. Downstream of the plate leading edge, the

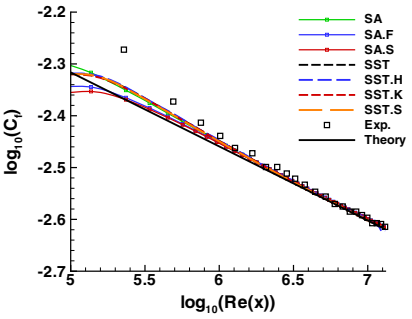

Fig. 1 Skin friction profiles, referenced to inlet conditions, are compared for the ZPGFP flow of Wieghardt [32]

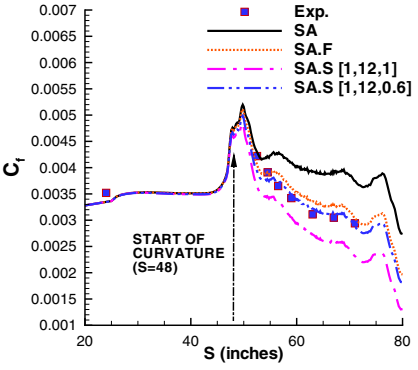

Fig. 2 Skin friction profiles, referenced to inlet conditions, are compared for the ZPGCCC of So [25] flow

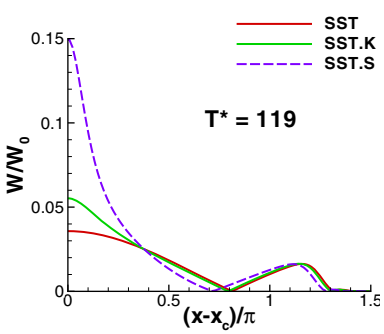

Fig. 3 Vorticity levels in a stationary isentropic vortex are compared after 199 turnover time scales for SST based VCMs

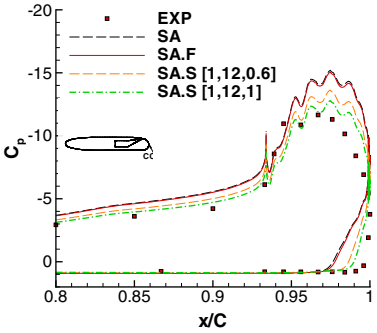

Fig. 4 Surface pressure along the circulation control surface are shown for the Novak flow [17]

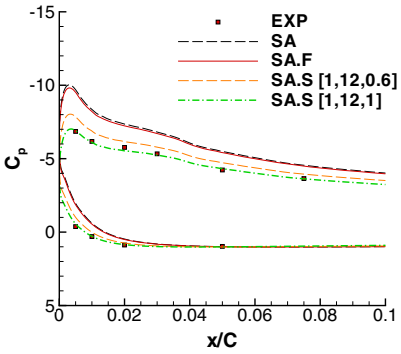

Fig. 5 Leading edge suction pressures are well predicted by SA.S for the Novak [17] flow

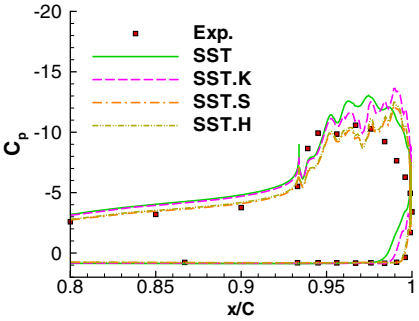

Fig. 6 SST based VCM's improve the estimation of the Novak CC surface pressure distribution. However all calculations severely overpredict the CCS suction peak in the separated flow region.

profiles agree sufficiently well with each other. For example, at $Re_x = 1x10^7$ the largest difference returned against the theoretical solution is given by SA.F at 0.12 percent and the smallest is returned by SST.S at 0.05 percent. The development of the shear stress profile at the plate leading edge is influenced by the SA based VC models, whereas the SST profiles are virtually identical. The SST solutions at the leading edge differ considerable from the theory up to about $Re_x = 1x10^6$, while the VC models bring the SA solutions into close agreement with the theory quite close to the plate leading edge ($Re_x = 1x10^5$). However, it is known that the turbulence models do not activate immediately at the plate leading edge, but rather at some finite distance downstream (which is a function of on-flow conditions [21]). The VC model response to convex curvature can be gauged by computing an attached

boundary layer flow over a convex surface (ZPGCC) [25]. Secondary flow and pressure gradient influences were carefully controlled in [25] so that only curvature effects are significant. The grid used is composed of 251x161 hexahedral elements with a maximum $y^+ \approx 0.3$ for the flow conditions specified in [25], [22]. Inflow profiles were specified according to [34] for the Spalart-Allmaras calculations. Figure 2 shows that while the SA model overestimates C_f over most of the curved wall, the SA.F profile produces better agreement with [25], and the best result is returned by SA.S with $C_3 = 0.6$. The SA.S solution shows considerable sensitivity to C_3 with a value of 1.0 significantly damping the computed skin friction below experimental values. Durbin [9] noted that turbulence in a boundary layer entering a convex curve is diminished due to the centrifugal acceleration - this has been confirmed by both the skin friction plot and examination of wall normal stress profiles not shown in the paper. The evolution of a stationary isentropic, with an initial solution corresponds to [30] is now examined. A uniform Cartesian mesh is used, composed of 25 6x256 elements, and covering a domain of $x \in [0, 10\pi]$, $y \in [0, 10\pi]$. The vortex is placed initially at the center of the domain and is then allowed to evolve for several turn-over time scales [8]. In figure 3, SST.S retains 15 percent of the original core vorticity while SST.K and SST solutions reduce by a factor of about twenty over approximately 100 turn-over timescales. This is due to the more accurate estimates of eddy viscosity that are returned by the VC models in the vortex core.

7 Applications to a Complex 2D Case

The ciculation control flow of Novak [17], with circulation jet momentum coefficient equal to 0.3, is discussed in this section. Others, for example Pfingsten et al. [18], have computed this flow using TAU and have showed that SA based VC models yield significant improvement in the prediction of surface pressure and wall-normal velocity profiles. In this section the sensitivity of the flow to the VC calibration coefficient is considered. The flow appears similar to that of the convex boundary layer flow however a better match is provided by $C_3 = 1$ for the SA.S VC model and this may reflect the increased contribution of pressure gradient effects for this flow as well as some sensitivity in the leading edge suction predictions to the VC model. Leading edge C_p profiles, presented in figure 5, return closest agreement with the experiment data with a choice of $C_3 = 1$ for the SA.S calculation whereas for $C_3 = 0$. the difference is higher. The SST based VC models show improvement for the flow in the CCS region, as seen in 6 however figure 7 shows that the SST based VC models underestimate the leading edge suction peak. Note that for the SST.S result the VC model is limited according to the recommendations of [24]. All VC calculations fail to correctly predict surface pressures in the separated flow region, due to a combination of grid and turbulence modeling defects which need additional study. Note that the solutions shown are properly converged, and the non-smooth behavior of the computed surface pressure upstream of the CCS separation of all solutions is due to a non-smooth local grid point distribution. The calculations

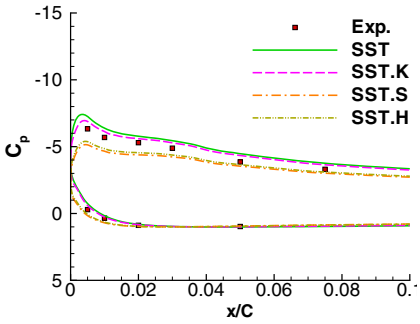

Fig. 7 The figure shows leading edge pressure profiles for the Novak flow returned ny the SST based calculations

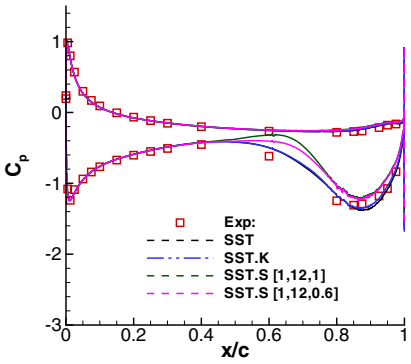

Fig. 8 Surface pressure profiles at 32 inches from root for the NACA0012 airfoil with rounded wingtip

demonstrate that the selection of the optimal VC model coefficient is still an open issue for complex flows and optimal values may be functions of the flow.

8 3D Cases

A proper review of validation computations on 3D configurations cannot be made in this short paper, but a brief review is made of current validation work. The VFE2 delta wing [6] [11] (at AoA=23 degrees)is being investigated to provide comparison of Hybrid-RANS and VC methods. This work will be reported in detail when it is complete. An interesting flow that is currently being examined is the flow of [5]. This flow is concerned with the roll-up of a wingtip vortex. Figure 8 illustrates surface pressure distributions taken at 32 inches from the wing root of the NACA0012 airfoil, which is the approximate location of vortex roll-up observed in the experiment of [3]. The SST and SST.K solutions match the experiment [5] well, but it can be seen that the vortex center returned for the SST.S solutions has moved in comparison to the SST and SST.K solutions: the vortex footprint is reflected in the surface pressure distribution which is substantially different. Note while some sensitivity to C_3 is seen in the figure, Smirnov et al. [24] reported that their implementation of the SST.C VC model requires a substantial reduction of C_2 from 12 to 2. Additionally some aspects of the vortical correction factor limitation implemented in the DLR TAU are different to those noted by [24]. Note that all inboard sections returned excellent agreement with experiment, suggesting that VC model calibration is a likely source of the discrepancies observed. The problems observed with the leading edge pressure distributions for the Novak case may also be resolved by a recalibration of VC model constants: appropriate choices for the SST VC model calibration are under further investigation. A observation with advanced VC models based on [29] is that optimum calibration values are flow dependent. While additional complexity

can be incorporated, doing so may violate the spirit of model simplicity and robustness necessary in the industrial environment.

9 Conclusion and Outlook

Tests on simple 2D flows indicate that vortical correction models perform as expected: reduction of turbulent stresses under conditions of convex curvature are validated and an improved persistence of vortex cores over long time scales is observed. In more complex 3D flows, pressure gradient and secondary flow processes impact on the flow evolution, leading to additional dependencies of the VC model calibration coefficients on the local flow physics. This suggests that if a notion of simplicity in VC model construction is be retained, there is a need for careful calibration of VC model constants for different types of flow, particularly in the industrial environment. The VM model of [29] is quite promising and appears to offer advantage over other approaches in one and two-equation RANS models.However, further validation in flows against rotating references frames and against Reynolds stress modeling is also required. This work is currently in progress and will be reported when completed. In conclusion the results obtained to date show expected behavior for the implemented VC models, but additional work is still required for an improved understanding of optimal VC model calibration coefficients.

Acknowledgements. This work was carried out within the internal DLR project RETTINA.

References

1. Batchelor, G.K.: An introduction to Fluid Dynamics. Cambridge University Press (1985) (reprint)
2. Bradshaw, P.: Effects of streamline curvature on turbulent flow. AGARD-AG-169
3. Bradshaw, P.D., Chow, J.S., Zilliac, G.G.: Turbulence measurements in the near field of a wingtip vortex. NACA TM 110418
4. Brandsma, F.J., Kok, J.C., Dol, H.S., Elsenaar, A.: Leading edge vortex flow computations and comparison with DNW-HST wind tunnel data. NLR-TP-2001-239 (2001)
5. Chow, J.S., Zilliac, G.G., Bradshaw, P.D.: Mean and Turbulence Measurements in the Near Field of a Wingtip Vortex. AIAA Journal 35(10), 1561–1567 (1995)
6. Chu, J., Luckring, J.M.: Experimental surface pressure data obtained on 65 delta wing across Reynolds number and Mach number ranges. NASA TM 4645 (1996)
7. Dacles-Mariani, J., Zilliac, G.G.: Numerical/Experimental Study of a Wingtip Vortex in the Near Field. AIAA Journal 33(9), 1561–1568 (1995)
8. Duraisamy, K., Lele, S.K.: DNS of temporal evolution of isloated turbulent vortices, Center for Turbulence Research. Proceedings Summer Program (2006)
9. Durbin, P.A., Pettersson Reif, B.A.: Statistical Theory and Modeling for Turbulent Flows. John Wiley and Sons Ltd. (2000)
10. Dwight, R.: Time-Accurate Navier-Stokes calculations with Approximately Factored Implicit Schemes. In: Groth, C. (ed.) Computational Fluid Mechanics, pp. 3–4. Springer, Heidelberg (2004)

11. Furman, A., Breitsamter, C.: Turbulent and unsteady flow characteristics of delta wing vortex systems. AIAA Paper 2008-0381 (2008)
12. Hellsten, A.: Some improvements in Menters $k-\omega$ SST Turbulence Model. AIAA-98-2554 (1997)
13. Hoffman, et al.: JFM (16) (1963)
14. Knight, D.D., Saffman, P.G.: Turbulence Model Predictions for Flows with Significant Mean Streamline Curvature. AIAA-78-258 (1978)
15. Menter, F.R.M.: Two-equation eddy-viscosity turbulence models for engineering applications. AIAA Journal 32(8), 269–289 (1994)
16. Moir, I.R.M.: Measurements on a two-dimensional aerofoil with high-lift devices. AGARD-Report AGARD-AR-303, vol. II, ch. A2 (1994)
17. Novak, C.J., Cornelius, K.C., Roads, R.K.: Experimental investigations of the circular wall jet on a circulation control airfoil. AIAA Paper 87-0155 (1987)
18. Pfingsten, K.C., Jensch, C., Körber, K.W., Radespiel, R.: Numerical simulation of the flow around circulation control airfoils. In: First CEAS European Air and Space Conference, Berlin (September 2007)
19. Pope, S.B.: Turbulent Flows. Cambridge University Press (2001)
20. Reynolds, O.: On the dynamical theory of incompressible viscous flows and the determination of the criterion. Philos. Trans. R. Soc. London Ser. A174, 935–982
21. Rumsey, C.L., Spalart, P.R.: Turbulence Model Behavior in Low Reynolds Number Regions of Aerodynamic Flowfields. AIAA Journal 47(4), 982–993 (2009)
22. Rumsey, C.L., Gatski, T.B.: Isolating curvature effects in computing wall-bounded turbulent flowa. AIAA 2001-0725 (2001)
23. Schwamborn, D., Gerhold, T., Heinrich, R.: The DLR TAU code: Recent applications in research and industry. In: European Conference in Computational Fluid Mechanics, Egmond aan Zee, ECOMASS CFD 2006 (2004)
24. Smirnov, P.E., Menter, F.R.: Sensitization of the SST Turbulence Model to Rotation and Curvature by Applying the Spalart-Shur Correction Term. Journal of Turbomachinery 131 (2009)
25. So, R.M.C., Mellor, G.L.: Experiment on convex curvature effects in turbulent boundary layers 60(1) (1973)
26. Synge, J.L., Schild, A.: Tensor Calculus. Dover Publications (1949)
27. Shur, M.L., Strelets, M.K., Travin, A.K., Spalart, P.R.: Turbulence Modeling in Rotating and Curved Channels: Assessing the Spalart-Shur Correction. AIAA Journal 38, 784–792 (2000)
28. Spalart, P.R., Allmaras, S.R.: A One-Equation Turbulence Model for Aerodynamic Flows. AIAA Paper 92-439 (1992)
29. Spalart, P.R., Shur, M.L.: On the Sensitization of Turbulence Models to Rotation and Curvature. Aerospace Science and Technology 5, 297–302 (1997)
30. Yee, H.-C., Sandham, N., Djomehri, M.: Low dissipative high order shock-capturing methods using characteristic-based filters. JCP 150
31. Widhalm, M.: TAU: Technical Documentation, DLR (2010)
32. Wieghardt, K., Tillmann, W.: On the Turbulent Friction Layer for Rising Pressure, TM1314M, NACA (1951)
33. Wilcox, D.C.: Turbulence Modeling for CFD. In: Wilcox, D.C. (ed.) DCW Industries (2002)
34. `http://cfl3d.larc.nasa.gov/Cfl3dv6/cfl3dv6`